ARMY RESEARCH LABORATORY

Real-Time Laser-Based Detection of Chemical Intermediate Formation in Liquid Propellant XM46 Shock-Loaded via an Electric Gun

by M. J. McQuaid, H. Burden,
and W. Lawrence

ARL-TR-1625 March 1998

The findings in this report are not to be construed as an official Department of the Army position unless so designated by other authorized documents.

Citation of manufacturer's or trade names does not constitute an official endorsement or approval of the use thereof.

Destroy this report when it is no longer needed. Do not return it to the originator.

Army Research Laboratory
Aberdeen Proving Ground, MD 21005-5066

ARL-TR-1625 **March 1998**

Real-Time Laser-Based Detection of Chemical Intermediate Formation in Liquid Propellant XM46 Shock-Loaded via an Electric Gun

M. J. McQuaid, H. Burden, and W. Lawrence
Weapons and Materials Research Directorate, ARL

Abstract

This report describes the development and results of an experiment designed to obtain real-time spectroscopic evidence of chemical intermediate formation in shock-loaded liquid propellant (XM46). Shock loads were produced by impacting small (<1 cm^3) XM46 samples with thin (0.075–0.375 mm) Mylar flyer plates. The flyer plates were accelerated to velocities near 1 mm/μs by the expansive forces of an exploding foil, a technique referred to as an "electric gun." A detailed description of the design of the gun developed for this study is provided. The performance of the apparatus was characterized in visualization experiments and via CTH (hydrocode) simulations. In spectroscopy experiments, the XM46 samples were probed at various delays following impact via laser-induced Raman scattering and fluorescence. A signature that may be attributable to NO_2 was observed, but cavitation was induced ahead of the shock wave, limiting our ability to establish the role of chemical intermediate formation in the shock-induced initiation of XM46. Issues in configuring experiments to detect chemical intermediate formation in shock-loaded samples via real-time, optically based spectroscopies are discussed.

Acknowledgments

The electric gun described in this report was built almost entirely from equipment loaned by U.S. Army Research Laboratory (ARL) staff members. We are particularly indebted to Drs. A. Birk, M. Miller, and C. Hollandsworth for their generosity. We are also thankful for the help of Ms. D. Pilarski, Ms. D. Saunders, and Mr. J. Trimble in configuring and running the experiments with the high-speed framing camera. Finally, we are grateful for the support and advice of Mr. J. Watson and Dr. R. Frey.

INTENTIONALLY LEFT BLANK.

Table of Contents

List of Figures

INTENTIONALLY LEFT BLANK.

1. Introduction

Reduction of propellant vulnerability through storage compartment design requires a knowledge of the mechanisms that can induce a violent propellant response. The work reported here was undertaken to support a Crusader (howitzer) development effort to establish design guidelines for fielding the liquid propellant XM46. A particular concern was shaped charge jet penetration of an XM46-filled container. Such an event will generate a shock wave that propagates through the propellant to container walls and possibly a free surface. The interactions produced at interfaces have the potential to generate (localized) high temperatures and cavitation [1–4]. Under certain conditions, XM46, which is generally very insensitive, will react explosively when subjected to such threats.

One of the primary methods for studying fundamental processes involved in a shaped charge jet strike has been flyer plate impact experiments [4, 5]. From the standpoint of understanding shock-induced initiation mechanisms, these experiments are preferred to experiments in which shaped charge jets are actually fired because they produce a nearly planar shock wave whose strength and duration can be well controlled and characterized. "Standard" flyer plate experiments conducted in support of the Crusader effort involved explosively launching a metal plate (with dimensions on the order of 150 mm × 150 mm × 10 mm thick) to velocities in the range of 0.3 to 2.0 mm/μs. Typical diagnostic approaches employed to follow the response of the impacted sample were piezoelectric pin arrays, which monitor the propagation (velocity) of the pressure wave, and high-speed photography. Based on such experiments, considerable progress has been made toward understanding the physical mechanisms leading to material initiation. The pressure wave velocity data was reduced to provide Hugoniot equation-of-state data [5], and it provided evidence for chemical energy release at high shock loads. High-speed photography provided a basis for identifying material failure and/or spall and the identification of reaction initiation sites.

However, these observations alone are not a sufficient basis for explaining the response of the propellant to a shock load. For example, in the standard flyer plate experiments, neither the shock wave velocity data nor the high-speed framing camera records indicate that XM46 changes

chemically when shocked to pressures less than 7 GPa, but the propellant will react violently when shocked to as little as 1 GPa if subsequently subjected to release and reshock [4]. The relatively long induction time observed between shock loading and rapid acceleration of materiel, coupled with the fact that propellant combustion is inefficient at pressures less than 10 MPa, indicates that the propellant decomposes to an intermediate chemical state that sets the stage for a violent reaction. Knowledge of such chemistry may suggest alternate approaches to reducing propellant vulnerability and may also be relevant to addressing the issue of long-term storage of XM46 that has been subjected to a strong, but noninitiating, shock load.

We were interested in whether shock-loading the propellant to between 1 and 5 GPa, by itself, was capable of inducing irreversible decomposition, and considered that this question could be answered via experiments in which a real-time, optically based spectroscopy was employed to detect chemical changes. However, because of the short temporal duration of such events, spatial considerations, the destructive nature of shock loading experiments, and the fact that there is little *a priori* knowledge of shock-induced chemistry, it is a challenge to develop an experiment in which high pressure transients are spectroscopically probed. A proven approach is the stepwise loading of a thin (O [250 μm]) sample impacted by a projectile accelerated via a gas gun. Nonenergetic materials loaded in this manner have been studied via infrared (IR) absorption [6], luminescence [7], and Raman-scattering [8] spectroscopies. In addition, the gas-gun approach has recently been extended to the study of energetic materials by Gupta and coworkers [9, 10], who investigated shock-induced intermolecular interactions in nitromethane via Raman spectroscopy. However, the exploratory nature of our investigation and the anticipation that a relatively large number of tests would need to be conducted, precluded the development of a gas-gun-based experiment, or, for that matter, trying to incorporate a laser-based spectroscopic probe into an explosively launched flyer plate experiment. The cost of tests involving a gas gun or explosively launched flyer plate would have been prohibitively expensive, running in the range of $500–$1,000 per test, and the construction of a gas gun would have also required substantial startup cost and time.

Based on a suggestion by Dr. Richard Beyer (U.S. Army Research Laboratory [ARL]), the search for an alternate shock-loading technique initially focused on laser-accelerated flyer plates. This

technique involves focusing a nanosecond or picosecond laser pulse onto a thin Mylar disk [11]. The pulse ablates material from the disk, creating a plasma that acts to accelerate it. The viability of coupling this approach with a spectroscopic diagnostic was demonstrated by Justus, Merritt, and Campillo [12], who reported results for the shock loading of 2,4-dinitrostilbene, and it is possible that a similar apparatus could have been constructed here. However, it was considered that the ability to quantify shock waves generated in this manner was limited, and that characterization of the shock wave on a test-by-test basis would have been onerous. Also, the maximum pulse energy of available lasers, which was on the order of 1 J, and the flyer plate velocities required (2 mm/μs), would have limited the study to the use of very thin (~0.01 mm) plates. Since the thickness of the plate establishes the duration of the shock pulse, it was questionable whether the results obtained in such tests could be extrapolated to understand the processes occurring in the "standard" flyer plate experiments.

The electric gun was identified as a potential shock-loading technique in the course of the literature search to assess the viability of the laser-accelerated flyer plate technique. The electric-gun technique is based on the fact that the discharge of a capacitor can deposit a large amount of energy into a foil via ohmic heating if the discharge time is short compared to the thermal diffusion time away from the foil. The deposited energy is released in the subsequent expansion of the resulting high-pressure and -temperature gas, which acts to drive a thin flyer (also referred to as a "slapper") positioned adjacent to it. Open literature articles discussing the electric-gun technique date from the early 1960s [13, 14], and a good review of the state of the art as of 1980 is provided by Chau et al. [15]. The technique has found application in establishing equation-of-state data, the study of shock initiation of explosives, and the characterization of shock wave—free-surface interactions. It has not, though, to our knowledge, been employed in spectroscopic studies of such processes. It allows the launch of much larger flyer plates (0.1 to 1 mm thick, 5–30 mm in diameter) than possible with a laser-accelerated approach, and velocities can (in principle) be calculated from the electrical-discharge current waveform using a calibration determined in separate experiments. This avoids the difficulty of configuring the experiment for the acquisition of spectral and imaging data in the same test. These factors led to our decision to pursue this approach.

This report provides details for the design, construction, and operation of the electric gun that we built. Although the articles on which we based our decision to proceed with an electric-gun-based approach outline considerations in gun design and performance, we found (by experience) that the articles gloss over or neglect various considerations that must be addressed if effective experiments based on this technique are to be realized. This report is intended to serve as a reference for future efforts that would benefit from the application of an electric-gun-based approach. Having been developed in an interdisciplinary effort and anticipating that its niche will be in similarly derived efforts, it is written at a level that will hopefully be accessible to a relatively wide audience. While it is not possible (or prudent) to provide all of the details and tradeoffs that go into building such devices, we have tried to include information sufficient enough for the reader to avoid most of the pitfalls inherent in electric-gun design and operation. Results of imaging experiments and CTH (hydrocode) modeling that characterize the performance and limitations of the constructed device are presented. Approaches for improving it are also proposed.

To probe for intermediate formation, a system to collect time-resolved Raman spectra was configured. The Raman effect is a well-known inelastic light-scattering phenomenon, producing frequency shifts ($\Delta\nu$) of incident radiation (ν) that permits species identification, and in favorable cases, measurements of the liquid's physical state [9, 12, 16]. Using a pulsed laser/optical multichannel detection implementation of this spectroscopic technique, a broad range of species can be surveyed within the short temporal window available to probe shock-loading processes. The laser pulse can also produce fluorescence, which may or may not be instructive. Evidence for NO_2 formation was observed in preliminary experiments, but imaging results indicate that cavitation was associated with the process. This issue is discussed, along with suggestions for future study.

2. Electric-Gun Design Considerations

The velocity that can be imparted to a flyer plate via an exploding foil depends on the foil material, foil and flyer plate mass/area, the nature of the current waveform, and the length of the barrel [13–15, 17]. Many of the decisions we made on setting these design parameters were based

on the availability of materials, previous experience with exploding wires, or recommendations in the literature. For example, although many different foil materials could have been employed, aluminum foils have been successfully used in this application, are inexpensive, and are readily available in a variety of thicknesses. Therefore, no other foil material was truly considered. The sizing of the sample and barrel was based on the paper by Chau et al. [15]. In particular, these researchers found that in order to achieve planar launch and flight, the barrel (and therefore flyer plate) needed to be at least 6 mm in diameter, and that the barrel length could not exceed 5 mm. The latter consideration limits the time available to accelerate the flyer plate to the desired velocity. Chau et al. [15] also recommended that the discharge burst the foil in less than one microsecond so that discharge-induced Lorentz forces would not distort the foil prior to its explosion. Such distortion would lead to a nonplanar launch.

At the time this experiment was being designed (i.e., the summer of 1994), the results of explosively launched flyer plate experiments were typically reported in terms of the initial pressure produced by the impact-induced shock wave, and reaction thresholds were associated with this pressure. (Alternate threshold criteria have since been proposed [18].) Based on these results, we were interested in developing an apparatus that could generate shock pressures in the range from 1 to 5 GPa. A simple one-dimensional (1-D) Hugoniot analysis indicated that to achieve pressures in this range with a Mylar flyer plate, the plate would have to be accelerated to a velocity in the range from 0.6 to 2 mm/μs. As a (conservative) goal, it was assumed that it would be desirable to launch 10-mm-diameter, 1-mm-thick plates (with a mass of 0.079 g) to 10 mm/μs. The kinetic energy for this case is 4 kJ.

In the subsections that follow, the design bases for the primary components of the electric gun that we built are discussed. The details of secondary systems related to safe operation, discharge characterization, and electrical noise reduction are given in the appendix. In many respects, the design and performance of our gun is similar to that described by Voreck and Velicky [17], who were trying to establish a shock sensitivity test to replace or supplement the NOL-Small-Scale Gap Test. A schematic diagram of our gun's discharge circuit is shown in Figure 1, and a schematic of the barrel-sample-container subassembly is shown in Figure 2.

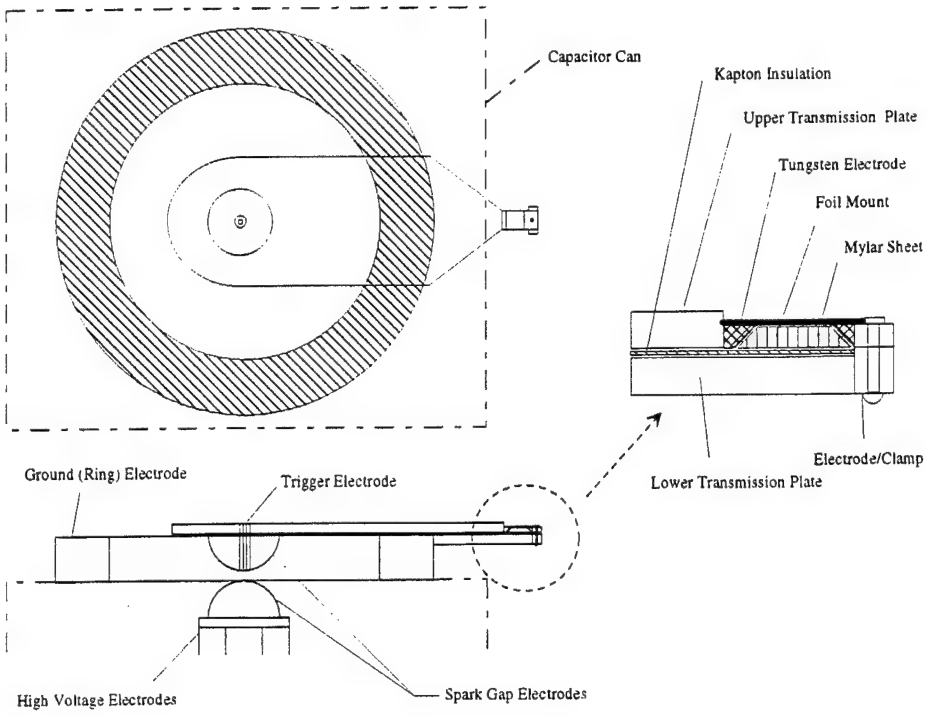

Figure 1. Schematic Diagram of Electric-Gun Discharge Circuit Components.

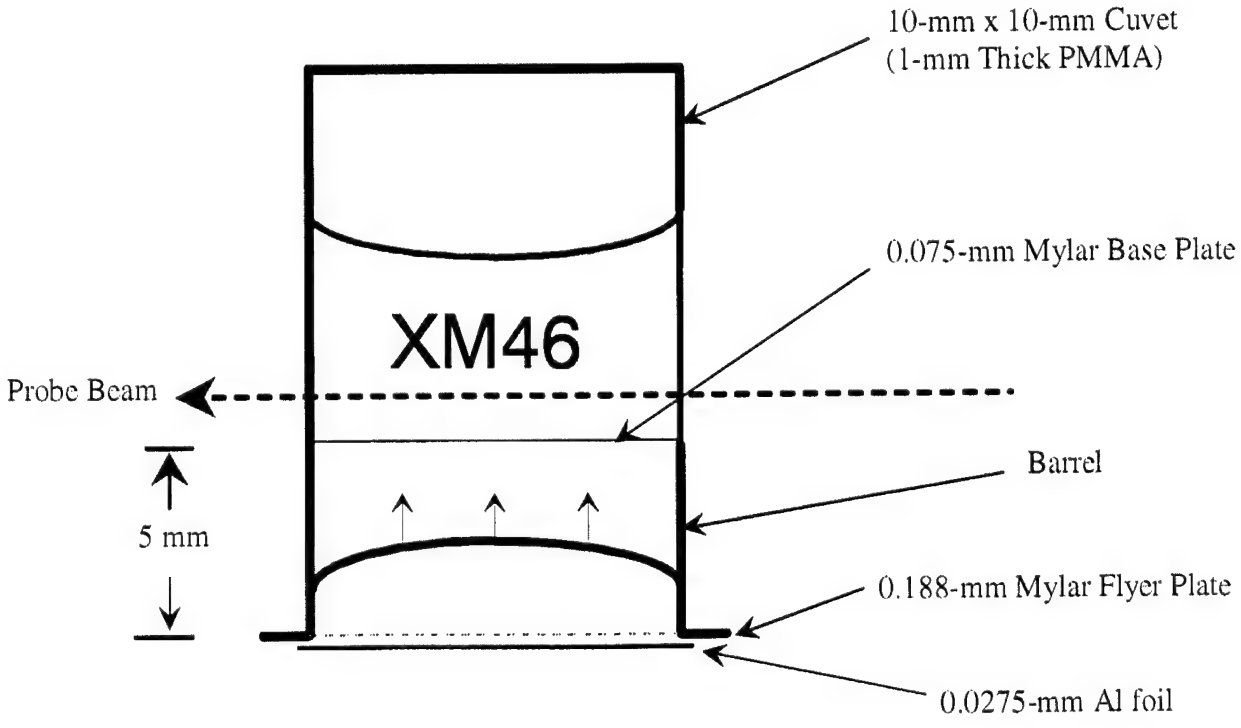

Figure 2. Schematic Diagram of Slapper-Barrel-Container Subassembly.

2.1 Energy-Storage Capacitor. The kinetic energy requirement and the limited time available to accelerate the slapper place implicit demands on the circuit's stored energy (E) and energy delivery time ($t \sim 1/f$, where f is the ringing frequency). In addition, the characteristic impedance (Z) of the system must be designed to ensure efficient energy transfer. Because $E = 0.5\ CV^2$, $t \sim 2\pi(LC)^{0.5}$, and $Z \sim (L/C)$, optimization of the circuit requires a trade-off between the energy-storage capacitance (C), circuit inductance (L), and capacitor charge voltage (V), and a computer program was written to assist in setting component values. Past experience with exploding wires served as a guide in estimating efficiency and determining the required electrical energy—efficiencies of between 85% and 90% having been achieved in converting electrical energy into a cylindrical shock wave by exploding a wire—and it was assumed that energy transfer from the exploding foil to the slapper would be of comparable efficiency. We later found that Guenther, Wunsch, and Soapes [14] reported efficiencies of 30% for one of their electric-gun configurations, and the electrical to mechanical energy conversion for our gun ended up being on the order of 10% for tests in which 1-mm/s velocities were achieved.

The best impedance match between the pulser and the rapidly changing load (associated with the heat-up and vaporization of the foil) was also estimated based on results obtained for wires. The best match for copper and aluminum wires has been found when the characteristic impedance is designed to be about 30 times the room-temperature resistance of the wire. The time needed to dump the energy contained in the storage capacitor to an inherently inductive circuit was taken as one quarter cycle of the oscillation frequency of the energy-storage circuit.

The primary variables that can be adjusted to achieve the needed energy while providing a satisfactory impedance match with the load (i.e., the exploding foil) are the capacitance and voltage rating of the capacitor. Also, because the time available to burst the foil is very short, and the rate of current increase is proportional to the ratio of charging voltage to inductance, circuit inductance must be minimized. Based on these considerations, a low-inductance (30 nH max.), 53-μF capacitor (Aerovox, Type PX80D36) with the capability of being charged to 44 kV (51 kJ) was chosen from among a number of models that were made available to us. Physically, the capacitor has coaxial terminals, the inner terminal being a 75-mm-diameter rod, and the outer terminal being a 25-mm-

thick ring with an inner diameter of 150 mm. The capacitor housing is a 30-cm × 37.5-cm × 56-cm metallic can equipped with mounting brackets. Weighing about 100 kg, it proved to be a suitable foundation for the rest of the gun.

2.2 Transmission Lines. The most efficient transfer of electrical energy to the foil is achieved when the load and source impedances are exactly matched. Mismatches between source and load impedances produce reflections that increase ohmic losses in the transmission line. However, since a range of foil thicknesses was to be tested, and the foil's impedance changes during the course of the discharge, precisely matching impedances is not possible. Therefore, the impedance of the transmission line was simply designed to be as low as possible. This was done by closely spacing parallel plates machined from 5-mm-thick aluminum stock. Also, the plates were made as short as possible, reducing the cumulative time for oscillations, and thus minimizing potential losses.

The upper plate of the parallel-plate pair was aligned and restrained by an insulating support structure that is described in the appendix. The lower plate was welded to a ring whose inner and outer diameters were similar to those of the ground (ring) electrode of the capacitor. Spacer bars were welded around the underside of the ring to lift the buswork such that the space between spark-gap electrodes was sufficient to hold off a 25-kV potential difference. Holes matching the threaded holes in the capacitor terminal were drilled through the ring and spacer bars to allow it to be bolted into place. Both of the plates forming the bus tapered from a width of 89 mm to 12.5 mm (the width of the foil ribbon) in a distance of about 50 mm. Edges of both plates were rounded to avoid high-voltage breakdown. The spacing and insulation between the plates was maintained by five 0.075-mm-thick sheets of dielectric film (DuPont, Kapton HV-300). The sheets were shaped so that they extended into the center area of the ring and about 75 mm on either side of the upper plate. This prevented current leakage and reduced the potential for carbonization and breakdown across the surface of the film.

2.3. Electrodes and Foil Mounting. For shot-to-shot consistency and the most uniform distribution of pressure over the flyer, it is essential to provide positive, uniform electrical contact over the width of the foil. Most of the designs reported in the literature accomplished this by

incorporating (sacrificial) electrodes and the foil into a laminate. For (perceived) operational convenience, we elected to incorporate a reusable foil clamp into the transmission plate/electrode design. The upper (high potential) transmission plate/electrode combination was positioned such that the end of the electrode extended about 2 mm out from under the support structure. The other electrode was a removable assembly that was secured to the lower (low potential) transmission plate by a screw that passed through a hole drilled in the clamp and a slot milled in the lower transmission plate. This arrangement allowed the spacing between the electrodes to be adjusted. Both electrodes were machined with 45° (downward facing) bevels that served to clamp a foil wrapped on a 1.6-mm-thick epoxy-fiberglass substrate mount. The ends of the mount were milled with upward-facing 45° bevels that mated with the beveled ends of the electrodes. Recesses were machined into the bottom face of the substrate to accommodate small lengths of foil folded over the beveled ends, allowing the mount to lie in firm mechanical contact with the dielectric film beneath it. The spacing between the electrodes was fixed by the width of the mount. For the testing that was performed, the width was chosen to be 12.5 mm, producing a square face that was slightly larger than the dimensions of the barrel (section 2.6). This arrangement was selected to reduce "edge effects"—the inherent nonuniform heating of a foil that results in the edges bursting slightly before the center. During loading, the foil-wrapped substrate is slid into contact with the fixed electrode, the adjustable electrode pressed firmly against it, and then tightened in place.

Because of imperfect contact, oxidation of surfaces, and the development of potentials due to electron (flow) acceleration as the flow transitions from the electrode to the reduced cross section of the foil, intense arcing occurred at contact points. This led to extensive erosion of the aluminum electrodes built and used in initial testing, prompting us to construct replacement electrodes from a tungsten alloy plate that was cut to the required dimensions with a low-speed saw equipped with a diamond-coated blade. The resulting electrodes were attached with screws to the upper transmission plate and to the adjustable clamp. Though it is more difficult to machine tungsten than aluminum, the improvement in electrode durability more than offset the extra machining effort required.

2.4 Foils. The foil thickness must be carefully chosen for a given capacitor voltage. If it is too thick, it will not burst quickly enough. If it is too thin, it will burst at too low a current to provide sufficient driving force. From the standpoint of a spectroscopy experiment, the latter is also a problem because the excess electrical energy is fed into the plasma, increasing background light emission. Preliminary testing was done with aluminum foils varying in thickness from 0.025 to 0.125 mm (1 to 5 mil), but, because of the added strain on system components produced by exploding thicker foils, most testing was performed with 0.0275-mm (1.1 mil)-thick foils. This foil thickness gave satisfactory performance when the capacitor was charged to 4 kV (400 J). Though well below the design goal of 4 kJ, preliminary testing indicated that 0.188-mm (7.5 mil) flyer plates were achieving velocities on the order of 1 mm/μs. This was considered reasonable for the purpose of shake-down testing and analysis. (The velocity measurement, though a rough estimate, indicates an electrical energy to kinetic energy conversion of about 10%.) Because of the time constraints imposed by the PM-Crusader program, we did not get an opportunity to explore the performance of thicker foils in any detail.

2.5 Flyer Plates. Flyer plates with the same dimensions as the inner wall of the barrel were formed from a 20-mm × 35-mm Mylar sheet by the barrel acting as a "punch" when the foil exploded. Mylar thicknesses in the range from 0.0625 mm to 0.375 mm (2.5 mil to 15 mil) were tested. To load the Mylar, it was placed on top of the foil with the back edge held between the electrode and the support structure. The front edge was clamped under the washer/nut combination used to secure the adjustable electrode. This was done to increase the inertial forces on the front and back edges, ensuring that these edges did not slide into the barrel, "short-circuiting" the punch out process. The large overhang on the side edges reduced the amount of luminous plasma gases reaching the field of view of the imaging or spectroscopic systems.

Early visualization results indicated that the nominal flyer plate velocities were in the range of interest, but that the flyers "ballooned" prior to being punched out into the barrel. After punch-out, the edges accelerated slightly relative to the center, but the disks were not planar at impact. Moreover, for plates ≤ 0.075 mm, the plasma gases broke through the film. Attempts were made to reduce ballooning by cutting (with scissors) "thick" (0.125 mm to 0.375 mm) Mylar sheets to fit

the inner dimension of the cuvet and sealing the barrel with a "thin" (0.0125 mm to 0.075 mm) Mylar sheet. However, this required considerable extra effort and yielded only marginal and hard to reproduce improvements. Therefore, efforts along these lines were discontinued.

2.6 Barrel and Sample Container. The search for an optically accessible sample container with dimensions on the order of 10 mm initially focused on using (cylindrical) polymethylmethacrylate (PMMA) tubing. However, the lensing/beam steering associated with this geometry is undesirable for a spectroscopy experiment, and "standard" PMMA has a short wavelength optical cutoff at about 390 nm. The latter consideration would have precluded a Raman study based on potentially advantageous 355-nm laser excitation. Thus we chose to use inexpensive ultraviolet (UV)-grade PMMA cuvets (Fisher Scientific) with 10-mm × 10-mm square cross sections that were expected to provide superior optical performance. It was also considered that the cuvets would make adequate barrels, and the design proceeded on this basis.

A schematic diagram of the slapper-barrel-sample-container assembly is shown in Figure 2. The cuvets were cut to desired lengths using a low-speed saw with a diamond-coated blade. As previously mentioned, the length of the barrel (5 mm) was based on work by Chau et al. [15] that indicated this was the maximum distance over which the flyer plate would remain parallel to the launch plane. The maximum distance was chosen since it allowed additional time for the flyer plate to accelerate. To provide an impact interface that was impedance-matched with the flyer, simplifying analysis of the impact process, the base plate of the sample container was constructed from 0.075-mm-thick Mylar sheet. Aluminized Mylar was employed when it was desirable to block the intense flash of the exploding foil from being transmitted up through the sample. The PMMA and Mylar were "tacked" together using a "welding" solvent. This solvent was also used to attach the barrel to the sample container. Transmission of the exploding foil flash through the barrel walls was blocked (when desired) by masking the barrel with black tape.

The assembly was placed on top of the Mylar sheet, (visually) centered over the foil, and butted up against the support structure. It was taped to the support structure to ensure good contact between the barrel and the Mylar and to provide positive positioning of the assembly. In addition, a small

metal bar was placed on top of the container, again to ensure good contact between the barrel and Mylar, but was also to prevent the flyer plate from striking and damaging the Plexiglas shield in tests in which a sample (which would normally brake the flyer) was not introduced.

2.7 Triggering Mechanism. In the interest of simplicity, compactness, and maintaining low inductance in the transmission line assembly, a Trigatron-actuated spark gap was employed for initiating the discharge of the energy-storage capacitor. The spark breaks down an air gap, which is otherwise sufficient to hold off the voltage, by producing UV radiation that (partially) ionizes the air. The spark-gap electrodes were essentially tungsten alloy bolts with hemispherical heads. The upper electrode, which contained a concentrically located trigger electrode, was screwed into the upper transmission plate. The lower electrode was screwed into the (internally threaded) center terminal of the capacitor. Coupled with washers, the height of the lower electrode could be adjusted to vary the width of the gap. The width was chosen such that it was sufficient to hold off the voltage difference between the center electrode and ground, yet would reliably break down for the same voltage when the spark was triggered. The design of the trigger circuit is described in more detail in the appendix.

2.8 Power Supply. Commercially built power supplies were used to charge the capacitor. The first unit employed was manufactured by Hipotronics (Model 825-100). This power supply is capable of charging the capacitor to 25 kV, and the voltage is read from a gauge on the unit. After the capacitor was discharged to explode the foil, an internal breaker would trip, preventing a recharge of the capacitor. The other power supply employed was a unit that was adapted from its intended application as an x-ray tube power supply (Field Emission, Model 314). A resistive load was incorporated into the charging circuit to increase the system time constant and prevent an overload condition during charging. Because the minimum increment of this unit's volt meter is 1 kV, a separate probe and digital (high impedance) voltmeter were employed to obtain an accurate reading.

3. Diagnostics

3.1 Discharge Characterization. Two devices were designed and built to characterize the electrical discharge: (1) a Rogowski coil to monitor the discharge current [19] and (2) a voltage divider to measure the instantaneous voltage across the foil. Together, these devices provided a measurement of the total energy imparted to the exploding foil. (The voltage divider was only employed in preliminary calibration testing.) The design and construction of these devices is provided in the appendix. The output of the Rogowski coil and the voltage divider were recorded on a digital waveform recorder (Nicolet, Model Pro 900).

3.2 Imaging. Visualization techniques were employed to characterize the flyer plate's acceleration and the dynamics of the impact process. Observations were first obtained using three intensified-charge-coupled-device (ICCD) cameras equipped with video lenses. A common controller was used to set the timing and duration of exposure for each camera. With this system, it was possible to obtain three 8-bit gray-scale images with exposures as short as 100 ns, and the interval between exposures was selectable (in multiples of 100-ns increments). Beam-splitting optics were employed so that each camera had the same field of view, and a 75-mm-diameter, 100-mm focal length lens was employed in front of the beam-splitting optics to optimize the projection of the image onto the ICCD elements. The flash from the exploding foil proved sufficient to obtain 100-ns exposures with the intensifier gain turned all the way down. This was fortunate since a Plexiglas shield (appendix) was required directly in front of the sample holder to protect the optical system, limiting our ability to provide external lighting. Also, increasing the gain of the intensifier increased image noise. The exposure was controlled primarily by the aperture setting of the video lenses. Neutral density filters were also occasionally employed to reduce light levels. The images were recorded on videotape and digitized via a personal computer (PC)-based frame grabber for further processing and analysis.

The images obtained with the ICCD cameras for times following slapper impact of the base plate proved difficult to interpret, motivating further visualization studies using a high-speed framing

camera (Beckman-Whitley, Model 189). This camera utilizes a gas-turbine-driven prism to control the exposure of a strip of 35-mm film. It is able to acquire 25 true-color images that have better resolution than those obtainable with the ICCD cameras. Operating the camera at an interframe time of 800 ns and exposure duration of 300 ns—times comparable to the ICCD camera system—the camera captured the event from start (foil explosion) to finish (the cuvet shattering). Further improvements in imaging were achieved by conducting the experiments in a blast chamber and employing large diameter collection optics that stood more than a meter from the experiment. This allowed the Plexiglas shield to be removed, permitting alternate lighting schemes to be employed. The search for better schemes was not extensive, though, and the only change to the original setup was the use of a small mirror to reflect the flash from the exploding foil back onto the sample. The downside to using the framing camera was that film processing delayed the availability of test results by about 1 day.

3.3 Spectroscopy. The primary components of the system employed to obtain time-resolved spectroscopic signatures were a pulsed Nd: YAG laser (Quanta Ray, DCR-10) and an optical multichannel analyzer (OMA). The laser output (1,064 nm, 25-ns pulse duration) was frequency doubled to produce 532-nm (ν = 18,790 cm^{-1}) radiation, allowing us to take advantage of better Raman-scattering efficiency (which increases ν^4) and placing the Raman spectrum in the wavelength range of maximum detector response. Some experiments with frequency-tripled output (355 nm) were conducted, and the results indicate that this approach is viable, but they are not presented or discussed here.

The laser beam has a torus-shaped spatial profile with an outer diameter of approximately 10 mm. To achieve reasonable spatial resolution, the beam was focused to a 0.5-mm-diameter waist using a 1-m focal-length lens. Since the Raman signal is linearly proportional to the incident laser power, the power (fluence) was raised to levels as high as practical with the given optical system. This proved to be approximately 10 mJ/pulse—a level above which the PMMA cell walls began to break down. There was concern that this fluence might be sufficient to photochemically degrade the propellant, but evidence that this occurred, such as the formation of bubbles or the appearance of new species in the spectrum, was not observed.

Light from the process was collected with a 50-mm diameter, f/1 condenser and focused onto the entrance slit of the monochromator (ISA, Model HR-320). The monochromator was equipped with a 600-grooves/mm grating (blazed at 500 nm) and a 1024-element, intensified photodiode array (Princeton Instruments, Model IPDA-1024). This system was operated in first order, with the grating positioned so that 532-nm (18,790 cm^{-1}) radiation diffracted just off the short wavelength edge monitored by the array. As such, this configuration surveyed radiation from about 535 nm (18,690 cm^{-1}) to 690 nm (14,590 cm^{-1}), and Raman transitions from 100 cm^{-1} to 4,100 cm^{-1} could be identified. To maximize throughput, the monochromator was oriented so that the entrance slit was parallel with the incident laser beam. Wavelength calibration was established by reference to the spectral lines emitted from a mercury vapor lamp. To reduce the effect of Rayleigh-scattered laser radiation, a long wavelength pass filter was placed in front of the monochromator entrance slit. Even so, the smallest $\Delta\nu$ that could be reliably recorded was 500 cm^{-1}. The detector was gated with a high-voltage pulser (Princeton Instruments, Model PG-100). The gate width was typically set to 18 ns and timed to onset at peak laser intensity. This approach yielded reasonable signal levels, while minimizing exposure to emission from the exploding foil.

3.4 Experimental Interface. Figure 3 is a schematic diagram of the experimental diagnostics and their interface with the electric gun. In initial testing with the ICCD cameras, the Trigatron-actuated spark gap was triggered with a manual switch, and the rise in the Rogowski coil output associated with discharge onset was employed to trigger a delay generator that acted to synchronize the instrumentation. (The actuation of the Trigatron itself was not chosen because the delay between activating the trigger transformer and the spark-gap breakdown was not reproducible, varying between 0 and 8 μs.) Triggering in experiments with the framing camera involved employing a trigger pulse from the camera to trigger a delay generator that actuated the spark gap approximately 10 μs before the prism was in position to expose the film. The uncertain (0 to 8 μs) delay between Trigatron activation and discharge onset was not a problem in this case because the length of the record was sufficient to allow for the variability.

In tests where synchronization of an ICCD image and a laser pulse was desired, the timing was complicated by requirements for achieving efficient, single-shot laser operation, namely that the

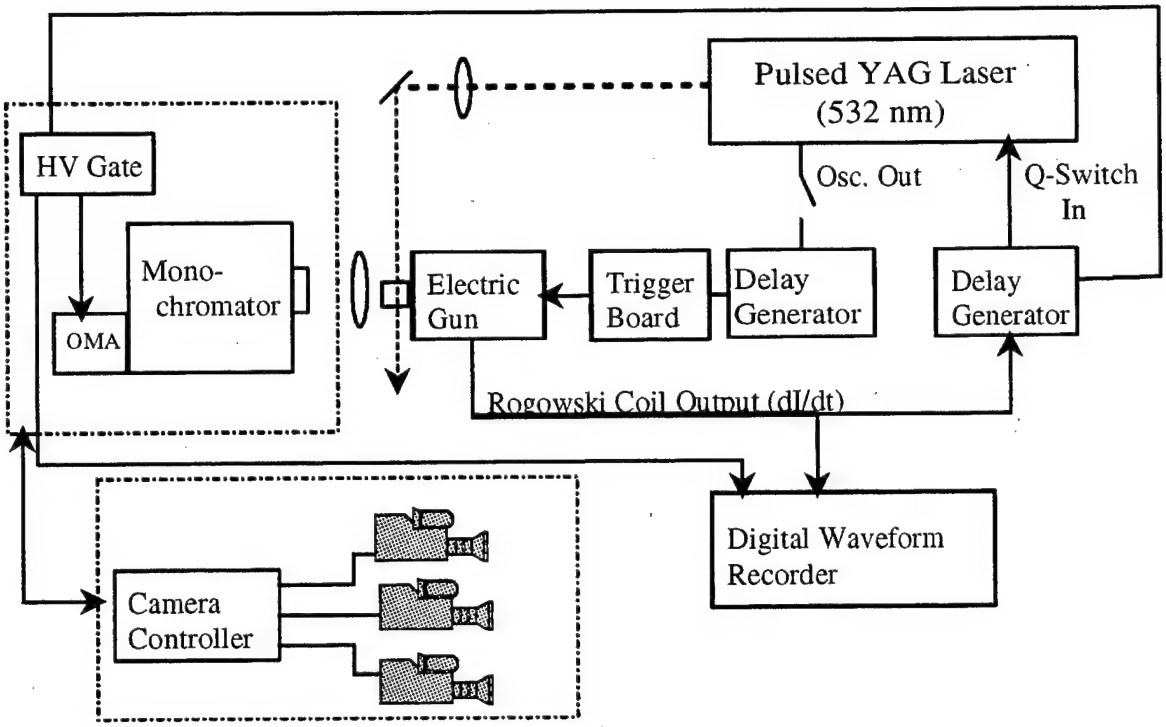

Figure 3. Schematic Diagram of Experimental Setup.

flashlamps be operated near 10 Hz, and that the Q-switch, which dictates when the laser pulse will actually be generated, be triggered approximately 210 μs after the onset of the firing of the flashlamps. This was accomplished by operating the laser on its internal clock and closing a manual switch to complete the circuit between an output of the laser-timing circuitry and a (master) pulse generator. The laser-timing circuitry triggered the pulse generator, which in turn triggered the discharge of the capacitor approximately 200 μs after the flashlamps were triggered, so that the desired evolution of the impact process was occurring at a time appropriate for the Q-switch to be triggered. The voltage rise induced in the Rogowski coil by the onset of the discharge triggered a second delay generator that controlled the timing of the Q-switch and the triggering of the ICCD camera controller. Monitors of the ICCD camera exposure and the Q-switch pulse (gates) were recorded on the digital waveform recorder. The triggering of the spectroscopy experiments was handled in similar fashion. Spectra were recorded directly to a PC.

4. Results

4.1 Discharge Characteristics. Figure 4 shows the instantaneous current and voltage values produced during a representative capacitor discharge. The evolution of the discharge involves four phases. The first phase is the heat up of the foil. During this phase, the resistance of the foil increases very little, and the current increases rapidly to its peak value of about 60,000 amps. The voltage across the foil rises in quasi-exponential fashion during this time. The second phase of the process is the melting of the foil. During this phase, the resistance of the foil increases moderately, and the current levels off. This phase is marked by a slope break in the voltage trace at 1.6 μs. The melt transition is a useful marker for testing the correlation between the measured energy and energy known to be deposited in a given weight of foil. The third phase of the process is the vaporization of the foil. At this point, only fine, widely dispersed droplets are available to conduct the current, and the resistance increases sharply. This is marked in the Rogowski coil trace by the instantaneous decrease in current at 2.0 μs. There are no signatures that mark the liquid-vapor transition or that characterize the heating of the vapor in the voltage record. The peak of voltage marks the point at which the last of the liquid metal is available for conduction. The delay between discharge onset and the burst of the foil was highly reproducible for a given set of parameters (voltage, foil thickness, etc.) and was in the range of 2 to 3 μs. Once the foil explodes, the vapor (usually) ionizes, and the resistance of the column drops. This is observed in the rapid drop in the voltage and the slow decrease of the current.

4.2 Imaging. Figure 5 shows a series of images obtained with the ICCD camera system at various times following discharge initiation. For these tests, 0.1875-mm (7.5 mil) Mylar disks were accelerated by exploding 0.0275-mm-thick aluminum foils with the capacitor initially charged to approximately 4 kV. These parameters were selected based on trial-and-error experimentation, and represented a trade-off between (1) achieving velocities near 1 mm/μs; (2) obtaining shock pulses that were as long as possible; (3) avoiding the "ragged" punch-out of thick (0.375 mm) plates; (4) avoiding the higher loads on the electric-gun electrodes produced by exploding thicker foils; and (5) optimizing the electrical energy coupled into the vaporization process, thus minimizing the

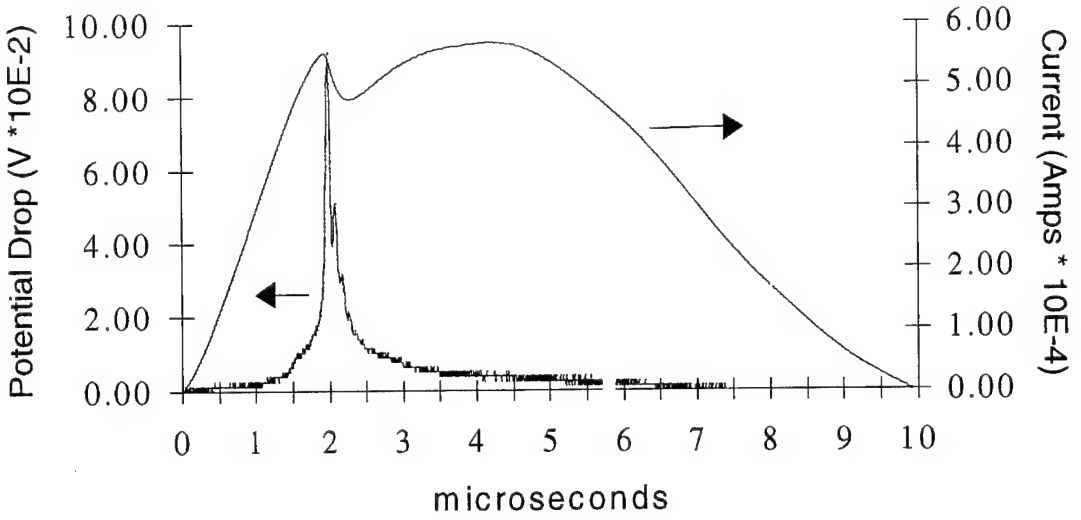

Figure 4. Integrated Rogowski Coil Output and Voltage Drop for a Representative Discharge.

plasma created by the dump of excess electrical energy into the aluminum vapor. Throughout most of the testing, a sample depth of 10 mm was (somewhat arbitrarily) chosen. Thinner samples were investigated toward the end of the program in an attempt to induce and observe surface displacement.

The flyer plate is observed to impact the divider at approximately t = 8 μs, about 5.5 μs after the foil burst. Ballooning of the Mylar is apparent. Bubble formation in the sample is also apparent at about this time. There was some variability in the results for subsequent times. Usually the propellant would turn "milky" and stay that way until after the cuvet shattered. (Optically clear cuvet shards with typical dimensions of several millimeters (or more) per side were recovered after tests, indicating that it was not the PMMA that was responsible for the milky appearance.) Occasionally there was a brief period during which the propellant clarified before turning milky again. In frames where the laser was fired while the propellant was bubbly or milky, intense scattering was observed. It should be noted that, although the cuvet shattered, there was never evidence of a violent propellant response. A slight scent of (what was assumed to be) NO_2 was apparent following the tests, indicating some fizz reaction did occur. However, it appeared that most of the liquid was simply dispersed in the containment area.

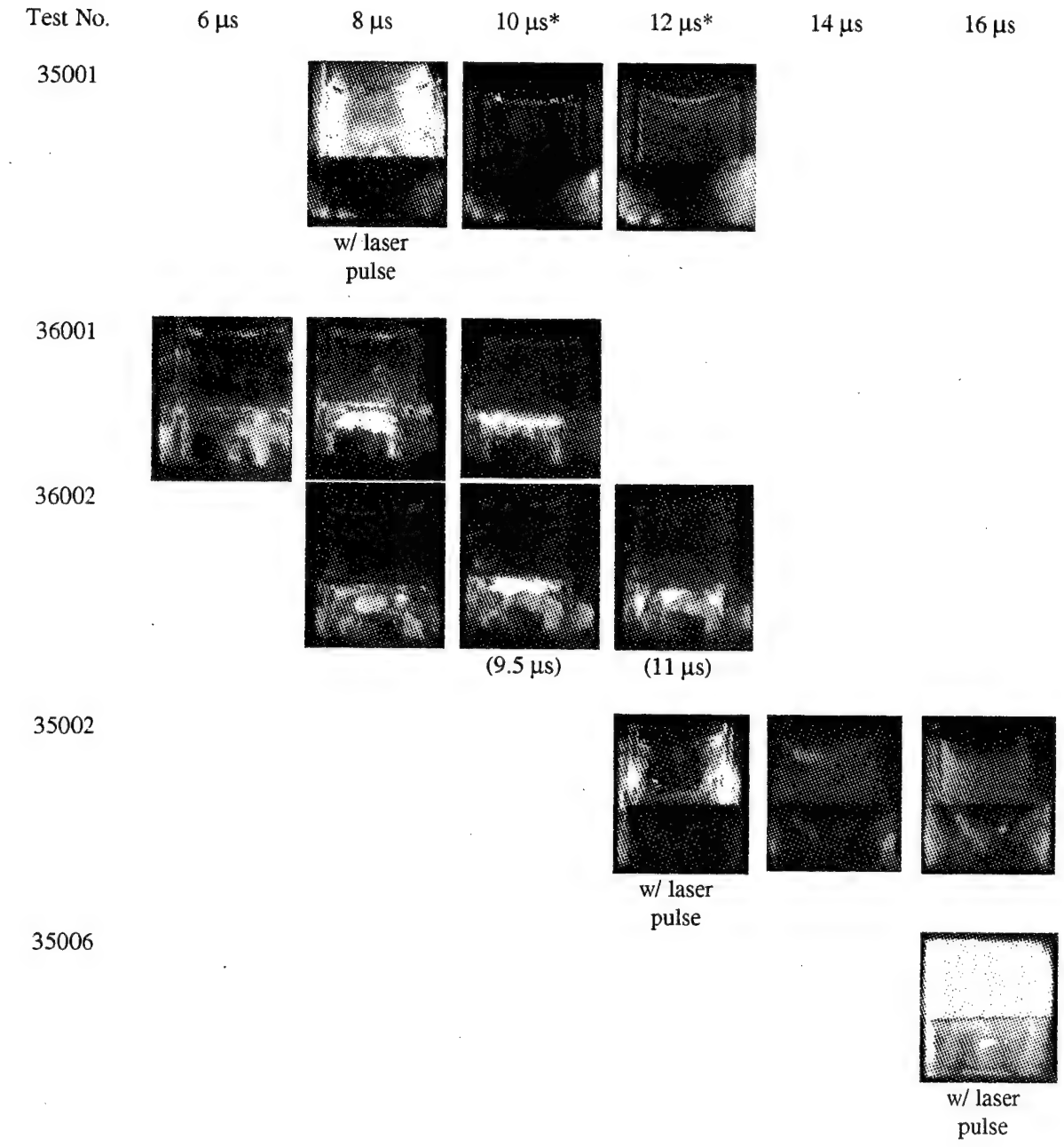

Figure 5. ICCD Camera Images of Representative Experiments.

The inability to directly observe the shock wave propagating through the liquid or establish the nature of the bubble formation prompted additional testing using the high-speed framing camera. Representative results are shown in Figures 6 and 7. The results shown in Figure 6 conclusively reveal that bubbles were forming in the liquid before the arrival of the impact-induced shock wave, indicating that a shock wave was being sent up the barrel walls ahead of the slapper. This wave was successfully decoupled from the process (Figure 7) by cutting staggered, thin horizontal slots into the barrel. However, this is as far as this experiment was developed when support for the PM-Crusader survivability workpackage was withdrawn.

4.3 Spectroscopy. A series of spectra acquired for various times following discharge onset is shown in Figure 8. The features at 17,740 cm^{-1} ($\Delta\nu$ = 1,050 cm^{-1}) and 15,390 cm^{-1} ($\Delta\nu$ = 3,400 cm^{-1}) are associated with the nitrate ion and water, respectively. These results are comparable to the HAN Raman signatures obtained under static conditions [20, 21]. The feature observed at 16,690 cm^{-1} ($\Delta\nu$ = 2,100 cm^{-1}) is considered to be associated with Raman-scattered radiation at 17,740 cm^{-1} that is scattered a second time. The emission associated with the flash of the exploding foil is shown for comparison. At a very cursory level of analysis, except for the broad feature that grows in at long wavelengths, all of the features are attributable to the propellant or emission from the flash. It was further observed that laser scatter from the bubbles swamp the detector at delays longer than 12 μs. (The spectrum at 12 μs is a typical signature produced by the OMA when exposed to intensely scattered 532-nm radiation. Why the OMA produces this specific response is unknown.) Based on comparison with spectra obtained from the slow, thermal decomposition of HAN in a diamond-anvil cell, it is considered that the feature that grows in at longer wavelengths may be associated with NO_2. However, due to the uncertainty regarding the nature of the process being probed, a more detailed reduction and analysis of the data was not pursued.

5. Discussion

5.1 Electric-Gun Performance. Although, based on our literature search, the electric-gun technique appears to offer a straightforward shock-loading approach that offers a good mix of cost and performance, the development of the gun is not trivial and would not have been feasible in the

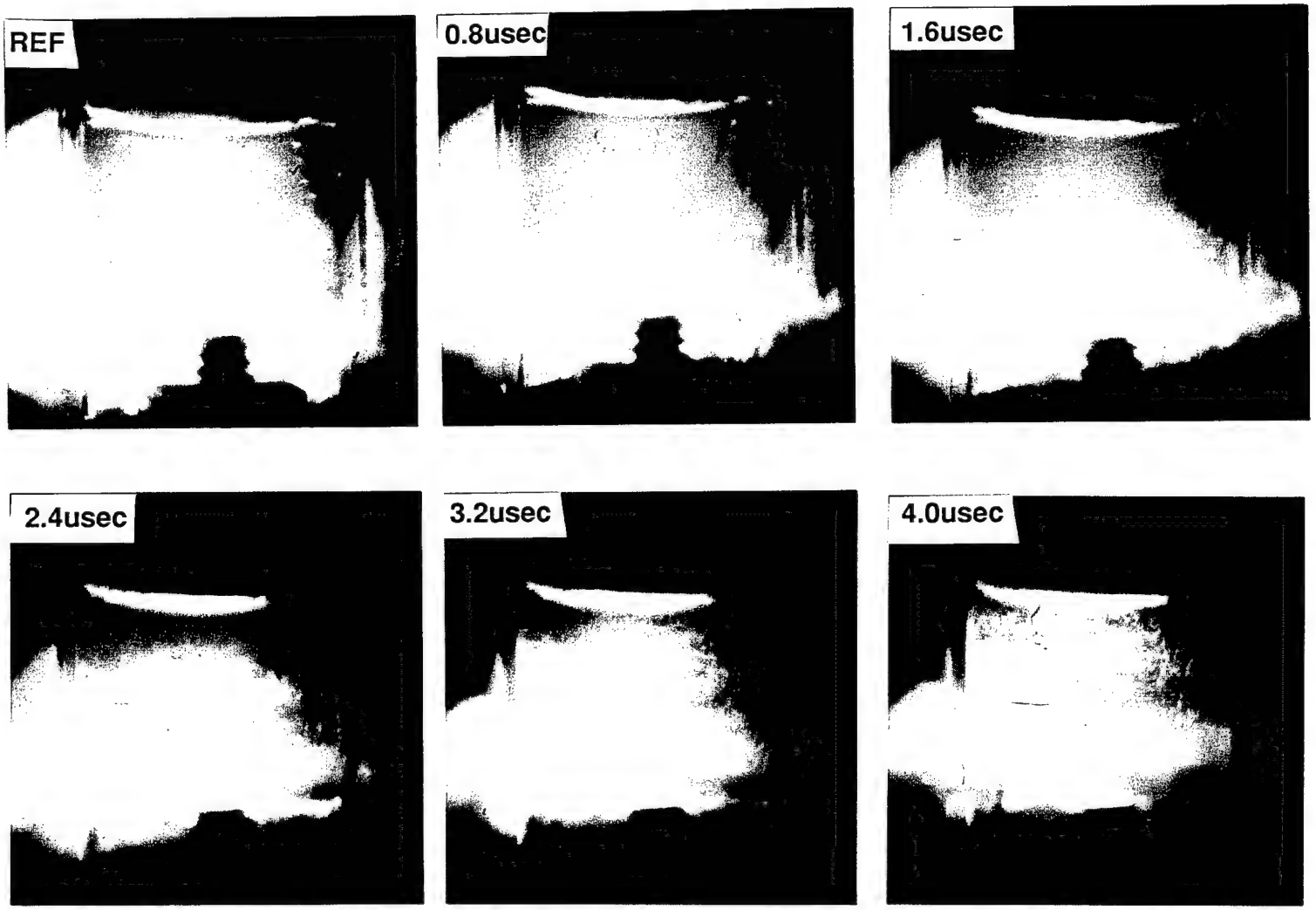

Figure 6. High-Speed Framing Camera Results Showing Bubble Formation Ahead of the Flyer Plate Impact.

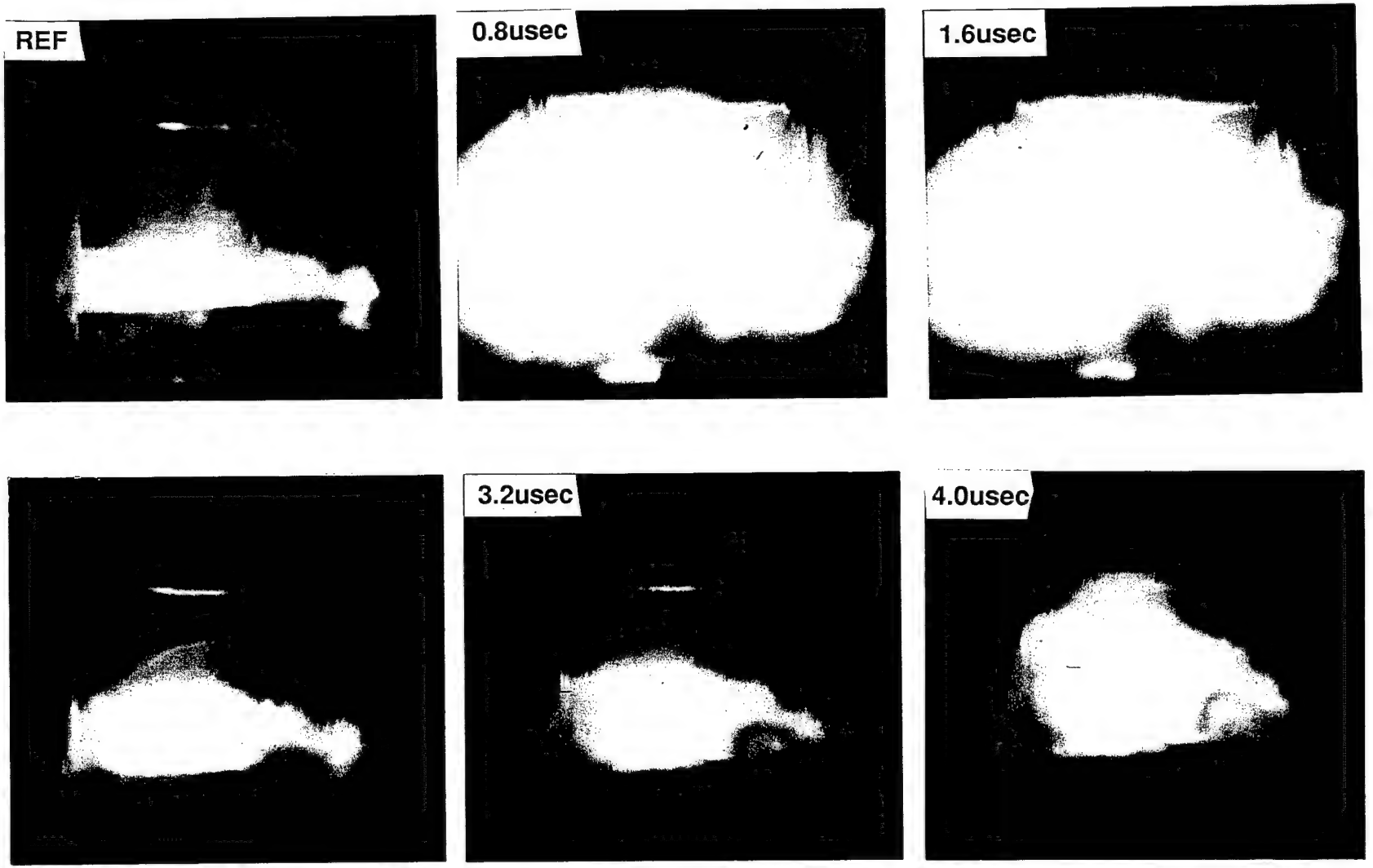

Figure 7. High-Speed Framing Camera Results Showing Shock Wave Propagation.

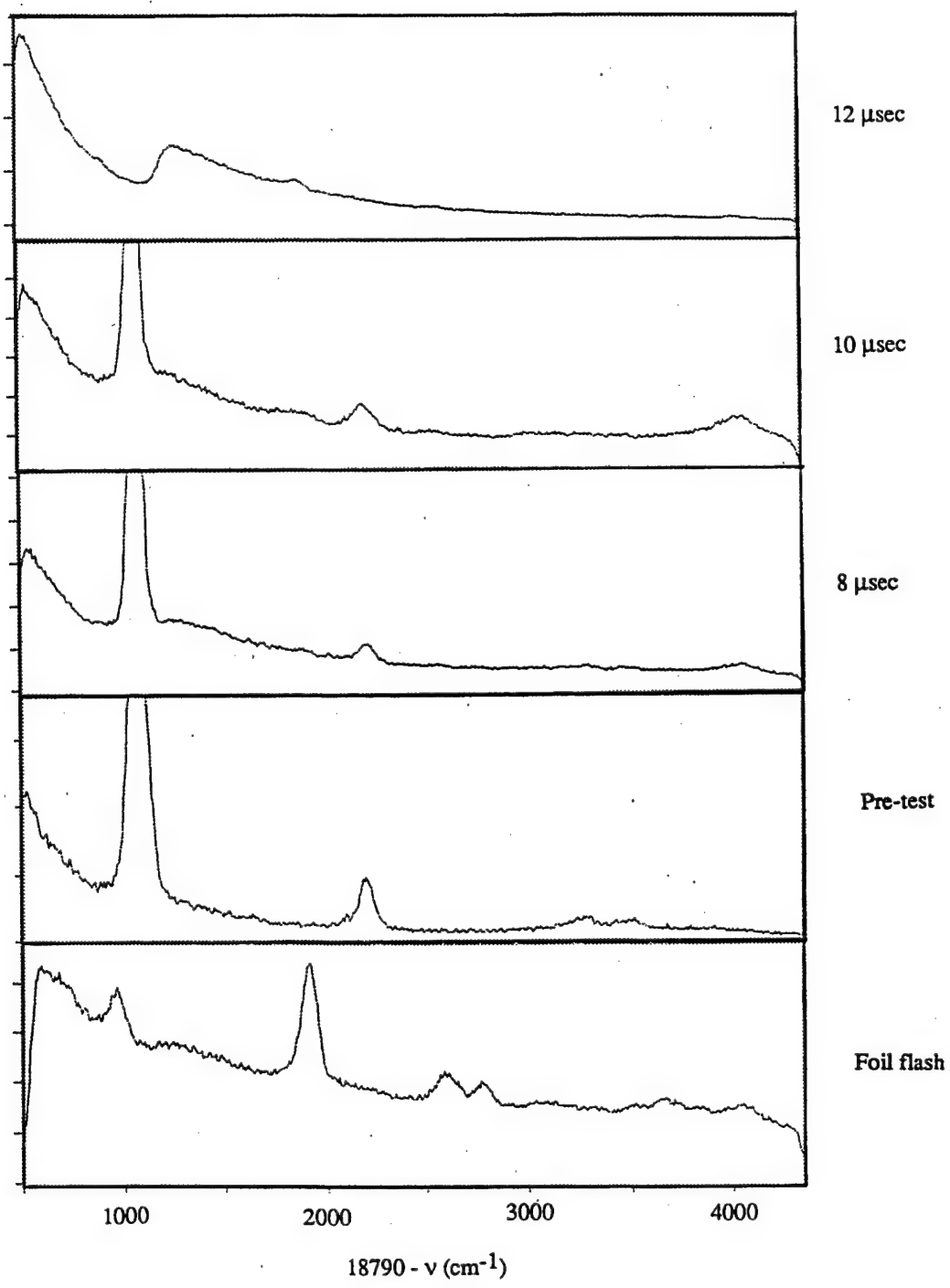

Figure 8. Spectra Obtained for Varying Delays Following Discharge Onset.

short time available under a PM-type development program without (1) much of the necessary equipment being already available and (2) the inhouse capability for engineering it. Much of this capability derives from ARL efforts to characterize capillary discharge phenomena related to electrothermal chemical (ETC) propulsion technology development. In retrospect, the decision to pursue this approach was risky, and it was only because of this existing capability that a reasonably successful device was built in 6 mo. This should be considered before a similar undertaking is attempted.

Beyond the technical difficulty of simply building the device, the literature available on the exploding-foil technique does not identify some of the problems that were encountered during the course of this investigation. In particular, we have not seen reference to the fact that a shock wave is sent up the barrel ahead of the flyer plate. In our case, the wave produced cavitation in the sample ahead of the flyer plate impact-induced shock wave—a situation that precluded us from studying the chemistry produced by shock loading in the absence of bubbles. This problem was overcome by cutting slots in the barrel, effectively preventing shock wave propagation up the barrel, but the program was ended before this remedy could be employed in spectroscopy experiments.

Also, despite following recommendations for achieving planar launch and flight, and constructing a device that was, in many respects, similar to those in the literature, extreme ballooning of the Mylar was observed. (It was thought that the recommendations addressed the issue of flyer plate tilt; the ballooning was a surprise.) The ballooning leads to the production of a shock process that is considerably more complicated than the planar process we were trying to achieve. This problem can probably be mitigated by redesigning the slapper and barrel assembly. The decision to employ the cuvet (and its square cross section) as a barrel was perhaps a mistake. The drag produced in the corners appears to contribute significantly to ballooning. As mentioned in section 2.4, some improvement was achieved by sealing the barrel with a thin plate and cutting the thick Mylar to the dimensions of the barrel. At a minimum, precise scoring of the flyer to facilitate the punch-out process should be performed. We would also reconsider employing a cylindrical barrel, since this geometry increases the area to circumference ratio and avoids localized drag. Also, the cylindrical geometry is simpler to model with a hydrocode.

In order to understand the ramifications of the nonplanar plate geometry and the influence of rarefaction waves from the container walls, the system was modeled with the CTH hydrocode [22]. Beyond characterizing the strength and duration of the shock pulse as it propagated through the sample, we were interested in the spatial and temporal window afforded for the spectroscopic probe. A simulation of the process produced when a curved Mylar flyer plate traveling at 1 mm/μs impacts the sample is shown in Figure 9. The result is qualitatively similar to that observed via the high-speed framing records (Figure 7). The simulation shows that (geometric) dissipation and rarefactions diminish the strength of the shock front, but establish that shock pressures in excess of 1 GPa were being achieved with the experimental technique.

These results are also pertinent in assessing whether the approach is capable of providing optical access following the release of a high-pressure transient. In experiments with gas guns, the whole (thin) sample is "shocked-up" and then released, and the probe radiation is transmitted through the entire sample. Here, the probe beam must be timed to arrive after the passage of the shock wave, but before secondary effects can operate. The imaging and hydrocode results suggest that access is available, but the spatial resolution is extremely coarse, and the (simple) identification of species will probably be the limit to which details of the chemistry can be elucidated.

Other challenges presented by the electric gun, perhaps addressed for the first time because of the intention to conduct a spectroscopic investigation, are related to precisely timing electronic instrumentation in the electrically noisy environment and the reduction of stray light from the extremely luminous flash of the exploding foil. The former were overcome by adherence to the guidelines given in the appendix. The latter were overcome by masking and electronic-gating techniques.

5.2 Spectroscopy. The ability to identify a chemical intermediate via Raman spectroscopy depends on the strength of its Raman-active transitions and its number density. Based on previous investigations of HAN decomposition [20, 23], it was thought that two species might be observed: (1) N_2O, which has a strong Raman-active transition at 1,285 cm^{-1} and (2) NO_2 which has a series of weak Raman transitions and a very broad fluorescence signal when excited at 532 nm. Either

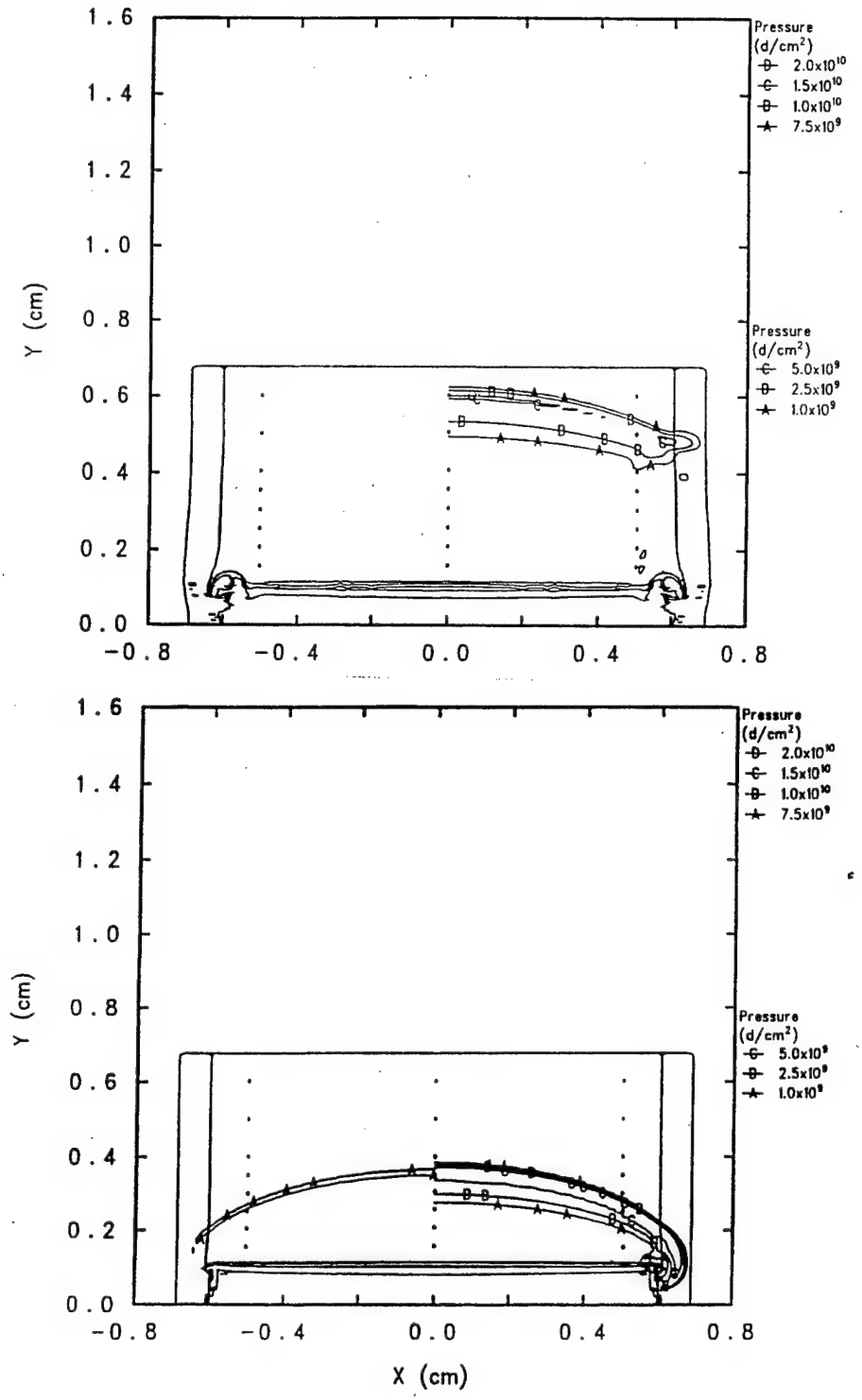

Figure 9. CTH Results. Shock Wave Propagation in XM46 Induced by an Elliptically Shaped Mylar Flyer Plate That Impacts the Base Plate at 1 mm/μs. Lower Figure Corresponds to 1 μs After Impact. Upper Figure Corresponds to 2 μs After Impact. For Each Figure, the Upper Pressure Key Corresponds to the Isobars on the Right-Hand Side, and the Lower Key Is for the Left-Hand Side.

would increase the sensitivity of the propellant, consistent with the increased sensitivity observed in shock-loaded propellant. The signal-to-noise level achieved in the preliminary experiments appears to be reasonable, and the results suggest the formation of NO_2, but the nature of the process leading to the signature is uncertain. N_2O was not observed, but the lower limit of detectability for this and other possible intermediates remains to be quantified.

The low-pressure thermal mechanisms for HAN decomposition proposed by Klein [23] suggest other species that might be detectable. It is thought that the first step in the decomposition of HAN is proton transfer from NH_3OH^+ to NO_3^- to produce HNO_3 (nitric acid) and hydroxyl amine or ammonia oxide. Moreover, nitric acid vapor is likely to decompose via the reaction

$$HO\text{-}NO_2 \rightarrow OH + NO_2. \quad (1)$$

One possibility for investigating NH_3OH^+ to NO_3^- proton transfer is to monitor the intensity or frequency shift of the N-OH stretch of NH_3OH^+ at 1,010 cm^{-1}. (There was not sufficient resolution in the current experiment to separate this feature from the strong NO_3^- symmetric stretch at 1,050 cm^{-1}.) Alternate diagnostic techniques for identifying HNO_3, hydroxylamine, ammonia oxide, and/or OH, species for which Raman scattering is perhaps not appropriate, might also be instructive.

6. Summary

An electric gun was designed and built as part of an effort to obtain real-time spectroscopic evidence for chemical intermediate formation during the shock loading of XM46. The gun is capable of launching 0.188-mm Mylar slappers to velocities near 1 mm/μs, and margin is available for producing more energetic impacts. However, some modification to the slapper-barrel-container assembly will be required in order to reduce ballooning of the slapper and to avoid shock propagation up the barrel ahead of the flyer plate. Laser-induced signatures were obtained, but cavitation was probably associated with the process, preventing us from determining whether chemical intermediates form in XM46 as a result of a shock load.

INTENTIONALLY LEFT BLANK.

7. References

1. Lyman, O. R., and J. T. McLaughlin. "Liquid Propellant XM46 Response to Four Different Shaped Charge Jet Attacks." ARL-MR-185, U.S. Army Research Laboratory, Aberdeen Proving Ground, MD, 1994.

2. Lyman, O. R., and O. H. Blake. "Liquid Propellant/Jet Interactions: Container Wall Effects." ARL-TR-670, U.S. Army Research Laboratory, Aberdeen Proving Ground, MD, 1995.

3. Gibbons, G., J. L. Watson, and T. C. Adkins. "Response of Liquid Gun Propellant to Shaped Charge Jet Impact." ARL-TR-1311, U.S. Army Research Laboratory, Aberdeen Proving Ground, MD, 1997.

4. Frey, R., J. Watson, G. Gibbons, V. Boyle, A. Finnerty, W. Lawerence, C. Leveritt. P. Peregino, D. Pilarski, O. Blake, A. Bines, and A. Canami. "Compartmentation Technology for Liquid Propellant (XM46)." ARL-TR-956, U.S. Army Research Laboratory, Aberdeen Proving Ground, MD, 1996.

5. Trott, B. O., H. N. Ebersole, and G. Fenton. "Hugoniot Equation of State and Direct Shock Response of Liquid Propellant XM46." *1994 JANNAF Propulsion Systems Hazards Subcommittee Meeting*, Chemical Propulsion Information Agency, 1994.

6. Duvall, G. E., K. M. Ogilvie, R. Wilson, P. M. Bellamy, and P. S. P Wei. "Optical Spectroscopy in a Shocked Liquid." *Nature*, vol. 296, p. 846, 1982.

7. Ogilvie, K. M., and G. E. Duvall. "Shock-Induced Changes in the Electronic Spectra of Liquid CS_2." *Journal of Chemical Physics*, vol. 78, p. 1077, 1983.

8. Schmidt, S. C., D. S. Moore, D. Schiferl, and J. W. Shaner. "Backward Stimulated Raman Scattering in Shock-Compressed Benzene." *Physical Review Letters*, vol. 50, p. 661, 1983.

9. Gupta, Y. M., G. I. Pangilanan, J. M. Winey, and C. P. Constantinou. "Time-Resolved Molecular Changes in a Chemically Reacting Shocked Energetic Material." *Chemical Physics Letters*, vol. 232, p. 341, 1995.

10. Pangilinan, G. I., and Y. M. Gupta. "Time-Resolved Raman Measurements in Nitromethane Shocked to 140 kbar." *Journal of Physical Chemistry*, vol. 98, p. 4522, 1994.

11. Ripin, B. H., R. Decoste, S. P. Obenschain, S. E. Bodner, E. A. McLean, F. C. Young, R. R. Whitlock, C. M. Armstrong, J. Grun, J. A. Stamper, S. H. Gold, D. J. Nagel, R. H. Lehmberg, and J. M. McMahon. "Laser-Plasma Interaction and Ablative Acceleration of Thin Foils at 1,012–1,015 W/cm^2." *Physics of Fluids*, vol. 23, p. 1012, 1980.

12. Justus, B. L., C. D. Merritt, and A. J. Campillo. "Efficient Photogeneration of Triplets in Shock-Compressed 2,4-dinitrostilbene." *Chemical Physics Letters*, vol. 156, p. 64, 1989.

13. Keller, D. V., and J. R. Penning. "Exploding Foils - The Production of Plane Shock Waves and the Acceleration of Thin Plates." *Exploding Wires*, W. G. Chace and H. K Moore (eds.), Plenum Press, NY, 1962.

14. Guenther, A. H., D. C. Wunsch, and T. D. Soapes. "Acceleration of Thin Plates by Exploding Foil Techniques." *Exploding Wires*, W. G. Chace and H. K Moore (eds.), Plenum Press, NY, 1962.

15. Chau, H. H., G. Dittbeener, W. W. Hofer, C. A. Honodel, D. J. Steinberg, J. R. Stroud, R. C. Weingart, and R. S. Lee. "Electric Gun: A Versatile Tool for High-Pressure Shock Wave Research." *Review of Scientific Instruments*, vol. 51, p. 1656, 1980.

16. Atkinson, G. H. "Time-Resolved Raman Spectroscopy." *Advances in Infrared and Raman Spectroscopy*, R. J. H. Clark and R. E. Hester (eds.), Heyden & Sons, London, 1982.

17. Voreck, W. E., and R. W. Velicky. "Exploding Foil Shock Sensitivity Test." *Proceedings of the Seventh Symposium (International) on Detonation*, 1981.

18. Fishburne, B., and P. Lu. "Safety Hazard and Vulnerability Assessment of XM46 Liquid Propellant." U.S. Army Armament Research, Development, and Engineering Center, Picatinny Arsenal, NJ, in press.

19. Pellinen, D. G., M. S. Di Capua, S. E. Sampayan, H. Gerbracht, and M. Wang. "Rogowski Coil for Measuring Fast, High Level Pulsed Currents." *Review of Scientific Instruments*, vol. 51, p. 1535, 1980.

20. Van Dijk, C. A., and R. G. Priest. "Thermal Decomposition of HAN at Kilobar Pressures." *Combustion and Flame*, vol. 57, p. 15, 1984.

21. McClaun, J. M., and S. L. Thomson. "CTH: A Three-Dimensional Shock Wave Physics Code." *International Journal of Impact Engineering*, vol. 10, p. 351, 1990.

22. Vanderhoff, J. A., S. W. Bunte, and A. W. Miziolek. "Laser Raman Studies Related to Liquid Propellants." BRL-TR-2657, U.S. Army Ballistic Research Laboratory, Aberdeen Proving Ground, MD, 1985.

23. Klein, N. "A Model for the Reactions of the HAN-Based Liquid Propellants." ARL-TR-405, U.S. Army Research Laboratory, Aberdeen Proving Ground, MD, 1994.

Appendix:

Auxiliary Subsystems of the Electric Gun

INTENTIONALLY LEFT BLANK.

This appendix provides design details for subsystems that do not directly relate to optimizing conversion of electrical energy into slapper kinetic energy, but are necessary for safe, reliable, and convenient gun operation. Also discussed are the design and construction of the Rogowski coil and the voltage divider employed to characterize the discharge waveform. Approaches to electrical noise reduction are reviewed.

A-1. Support Structure. The electrical discharge results in large magnetic (Lorentz) forces that tend to drive the closely spaced parallel transmission plates apart. We calculated that a current of 434,000 A would be produced if the capacitor was charged to 10 kV and (accidentally) short-circuited. This would generate a force of 108,000 N on the 25-mm-long, 12.5-mm-wide rectangular section of the transmission lines. To prevent the plates from separating, which among other things, would lead to a loss in thrust, a support structure was required. Moreover, to avoid short circuiting the foil, this structure had to be constructed from insulating materials. Material available for the construction of the support structure was a 25-mm × 125-mm "Bakelite" laminate having a nominal modulus of 1.4×10^{10} N/m^2. For the 27.5-cm lengths required to span the capacitor (ring) terminal, it was estimated that the force applied continuously to the 25-mm-wide surface would deflect the beam 6 mm, producing a material failure. However, because the force would be applied in less than 10 μs, the support is massive, and the magnetic force would fall rapidly as the distance between the plates increased, we elected to proceed with this material.

To complete assembly of the structure the cross members were bolted ladder-like between the webs of two 20-cm wide fiberglass channel beams. The flanges of these beams were bolted to the capacitor's mounting lugs. One cross member, located across the spark gap, supported the upper plate of the line and maintained the spacing between the spark-gap electrodes. A second member above the upper plate restrained it where the lower plate began. The third restraint, consisting of a contiguous pair of members, supported the entire narrowed portion of the upper plate. The narrowed portion of the lower plate, being near ground potential, was restrained by a massive aluminum cross member directly under it.

A-2. Dump Resistor. A capability for safely "dumping" charge from the storage capacitor was needed because not all of the initially stored energy was discharged during the transient to burst the foil—up to 500 V being routinely left on the center terminal. Such high voltages would have, at a minimum, created arcing and sparking when engaging the (low resistance) shorting device (section A-3), and probably would have welded it to the capacitor terminals. To provide a dump capability, a separate path to ground was provided by a line containing a dump resistor. The dump resistor was also needed (and designed) for the more demanding possibility of the capacitor being charged to a high value for a shot and the shot needing to be aborted. In this case, up to 25 kV (16 kJ) might have to be discharged.

The primary criteria for a safe dump is that the discharge be slow enough to prevent arcing and sparking (i.e., on the order of seconds). The rate of decay for an RC circuit is given by

$$V = V_o e^{-t/RC}, \tag{A-1}$$

where V_o is the initial voltage, C is the capacitance (in farads), and R is the resistance of the dump resistor (in ohms). Since the time constant for the discharge is proportional to RC, and a minimum discharge time of about 5 s was sought, a time constant (τ = RC) of about 1 s was required. (With a time constant of 1 s, the voltage drops to 0.6% of its initial value in 5 s.) With the storage capacitance fixed at 53.12 μF, a 18,825-Ω resistance is required to obtain such a value.

Since it is important that the energy to be dissipated not be larger than the resistor's thermal capacity, the dump resistor designed for this application took the form of a flexible plastic tube filled with a conducting (sodium chloride/water) solution, and the cross-sectional area of the tube and its length were adjusted to give the proper resistance and thermal capacity. For a constant resistance, any increase in conductive cross-sectional area must be compensated for by an increase in length. To limit the temperature rise (ΔT) to 20 K, the mass (m) of solution required is

$$m = \frac{Q}{c\Delta t}, \tag{A-2}$$

where Q is (conservatively) equated with the energy contained in the charged capacitor (16 kJ at 25 kV), and c is the heat capacity for water (4.2 kJ/kg). Substituting these values into equation (A-2) yields a mass requirement of about 0.2 kg.

One gram of sodium chloride in 0.2 kg of water produces a solution having electrical resistivity (ρ) of 1.50 Ω-m. The resistance and thermal capacity are both functions of the length (l) and cross-sectional area (A), viz.,

$$R = \frac{\rho l}{A}, \tag{A-3}$$

and

$$m = \partial l A, \tag{A-4}$$

where ∂ is the density of the solution. Rearranging equations (A-3) and (A-4) to find A in terms of ρ, m, R, and ∂ yields

$$A = \sqrt{\rho m / R \partial}, \tag{A-5}$$

Substituting in appropriate values, A is found equal to 1.26 cm^2. Such a cross-sectional area is conveniently provided by tubing with an inner diameter of 1.25 cm. The required length (1.58 m) is then found via equation (A-3) or (A-4).

To assemble the resistor, cylindrical brass plugs were employed at each end of the tube to serve as corrosion-resistant electrodes. The plugs were axially drilled and tapped to accept brass screws that served to provide lead connections. One of the plugs was drilled all the way through to provide a vent for air bubbles. A fiber washer under the terminal lug on this plug prevented leaking. Hose clamps at the ends of the tube held the plugs firmly in place. The resistor was connected in series with a relay that was closed to complete the path to ground. To ascertain whether residual charge was successfully dumped, the voltage reading would be observed as the relay was closed. Proper operation was associated with a "slow" (several second) decline of the voltage (reading) to zero.

A-3. Shorting Device. A device to place a direct short-circuit across the capacitor after it is discharged through the dump resistor was incorporated into the design. It consisted of an aluminum strip that was bent to make sliding contact with the capacitor's outer (ground) ring, while simultaneously making a direct, spring-loaded contact with the center (high voltage) conductor. This strip was attached to the lower end of an insulating rod. The bottom of this rod fit into a shallow depression in the capacitor's ceramic insulator. At the top of the rod, an insulating handle was attached. The handle allowed the rod to be rotated to engage (or disengage) the contact. When disengaged, the entire assembly could be lifted clear of the high-voltage elements of the pulser and rotated to rest on a support. When the assembly was lowered and rotated into contact, a screw extending from the underside of the handle engaged a spring detente that maintained the contact. This provided an easily confirmed, visual assurance that the equipment was discharged and safe to work on.

A-4. Screen Enclosure. A screen enclosure was constructed from a single piece of aluminum window screen. The primary purpose of this enclosure is to intercept the changing electric fields produced by the discharge that could otherwise couple into the surroundings, creating electrical noise. A secondary, but valuable, function of the enclosure is to prevent personnel from accidentally accessing high-voltage elements. The enclosure was a five-sided box, with an opening in the top to accommodate the shorting mechanism. The front could be opened for access to the experiment. A strip at the bottom of each side was folded under the channel beam-to-mounting lug bolts, clamping the screen and grounding it to the capacitor case. Tabs on the back side of the box were also clamped under the rear tie-down bolts. Holes for optical access were cut in the front and one side without noticeably compromising the enclosure's effectiveness.

A-5. Protective Shield. For tests conducted in the laboratory (as opposed to the blast chamber), a transparent L-shaped shield assembled from 9-mm-thick Plexiglas was installed to contain shrapnel. The shield was held between the fiberglass beams of the support structure (section A-1) by removable pins inserted through the web of the beams. Despite its close proximity to the experiment, the front face of the shield suffered only minor scratches over the course of this study. The top section of the shield was damaged by the flyer if the flyer did not impact a sample or some

other stop. In experiments where 355-nm laser excitation was employed, a hole was drilled in the shield, and a window was installed that could pass near-ultraviolet (UV) wavelengths.

A-6. Rogowski Coil. A Rogowski coil is a device that effectively integrates the magnetic field over a path surrounding a current-carrying conductor. The device works in accordance with Ampere's circuital law, which states that the line integral of the magnetic field intensity around any enclosed path is proportional to the total current flowing in an encircled conductor. Each individual turn of the helical winding encompasses some of the magnetic flux lines surrounding the conductor. The cumulative effect of the turns of the winding, when it is formed into a circular configuration, emulates the line integral and proves effectively insensitive to its location and orientation relative to the conductor. To preclude the circular configuration from becoming a completely closed, highly orientation- and position-sensitive loop, the signal-lead shield was attached to the beginning of the helix, and the center conductor was fed axially through the entire helix and attached to the end. The rate of change of the magnetic field intensity is proportional to di/dt, where i is the current in the conductor and produces an output voltage in the helix whose integral with respect to time is proportional to the current

$$V = \frac{0.25\ \pi\mu_o n d^2}{l}(di/dt), \qquad \text{(A-6)}$$

where μ_o is the free space permeability ($4\pi \times$ N/A^2), n is the number of turns in the coil, d is the mean diameter of a helix turn, and l is the mean circumference of the loop. The instantaneous values of current are obtained by integrating the recorded values.

In order to design a coil that will produce a full-scale response for the anticipated operating conditions, values for gun-specific parameters need to be estimated. The dimensions of the capacitor dictated a loop diameter of 19 cm (l = 60 cm), providing a separation from circuit conductors sufficient to avoid serious alteration of the turn-to-turn capacitance or inductance of the coil. The peak value of di/dt was estimated by dividing the anticipated maximum charge voltage (32 kV) by the inductance of the plates in the storage capacitor (30 nH), yielding a value of 1.067×10^{12} A/s.

Rearranging equation (A-6) yields

$$nd^2 = \frac{4V_o l}{(\mu_o \pi \, di/dt)}, \qquad \text{(A-7)}$$

where V_o refers to the maximum full-scale reading of the voltage measuring device. For the digital waveform recorder employed in this study, V_o is 20 V. With this value and the gun-specific values previously estimated, nd^2 is found to be 1.14×10^{-5} m^2. With n assigned an arbitrary value of 25 turns, the mean diameter of each turn would need to be 0.68 mm. We did not think that we could make this value with the needed precision. Therefore we decided to employ a 10X attenuator on the oscilloscope input, increasing the maximum measurable output voltage to 200 V and increasing the optimum mean turn diameter to 2.14 mm.

To build the coil, the fluted end of a drill bit was chucked in a lathe and one or two turns of no. 20 AWG wire were wound on the unfluted part. The lathe was turned by hand until 25 turns were in place; winding progressed toward the chuck, and each new turn slid the coil toward and off the end of the drill bit. The coil produced in this manner was then stretched to the desired length. The proper size was found by trial and error, different bit sizes being employed until the mean diameter (the outer diameter minus the wire diameter) of the stretched coil was near the desired value. The jacket and shield were stripped off a section of a length of RG-273/U cable, and the center conductor of the cable was threaded along the axis of the coil and soldered to its end. The other end of the coil was soldered to the cable shield. The cable and its connector passed through a 6-mm hole drilled in a lower bus ring spacer bar. The two ends of the coil were then brought together physically (though electrically insulated) and fastened to form a loop.

To calibrate the Rogowski coil, its response was compared to that of a commercially built and calibrated (and more sensitive) current transformer (Pearson Model 101). The calibration tests involved stringing the leads of both devices to an air-core coil (several turns, 0.3-m diameter) into which a capacitor was discharged. For comparison, the voltage output of the Rogowski coil had to be integrated with respect to time.

A-7. Voltage Divider. A 100:1 voltage divider was built to measure the instantaneous values of voltage across the foil during a discharge event. Together with the Rogowski coil measurements, these data provide information on the power transferred to the foil. The divider was constructed from 11 90-Ω and 1 10-Ω carbon resistors. For undistorted response, it is desirable to keep the ratios of each of its elements' resistance, inductance, and reciprocal capacitance the same. However, for this arrangement, the ratio of inductances was about 12:1, and the ratio of capacitances was on the order of 1:12. To increase the latter ratio, a conductive foil touching one lead was wrapped around the small output resistor. A hole the size of a resistor lead was drilled in the upper transmission line as close as possible to the end of the electrode. The lead from the chain formed by the series-connected 90-Ω resistors was forced into this hole, and the chain was laid in a rectangular path—moving, first, away from the transmission line to avoid explosion products and any likelihood of arcing, then bent to run parallel to the exploding foil, and, finally, bent to return close to the line where it joined the 10-Ω resistor. An adjustable spring made contact with the clamp that secured the grounded end of the exploding foil. The oscilloscope input was connected across the 10-Ω resistor. Because the resistor chain formed a loop, it detected both the resistive and the inductive components of voltage developed across the exploding foil. To determine the inductance of the loop, the pulser was discharged with a massive, very low-resistance conductor, developing an almost entirely inductive voltage (V_c). Coupled with the di/dt values derived from the Rogowski coil, the inductance can be computed via the relationship

$$L_c = V_c/(di/dt)_c . \tag{A-8}$$

The voltage across a foil (V_f) can then be related to a recorded voltage (V) using

$$V_f = 100[V - L_c(di/dt)] . \tag{A-9}$$

The product of the current and the voltage gives the instantaneous power being generated. A time integral of the power traces the expenditure of energy used in heating, melting, and, finally, vaporizing the exploding foil. Thus, it served to establish the efficacy of the circuit design. Once established, the performance of the gun could be determined from the Rogowski coil data alone.

A-8. Triggering Mechanism. A commercial trigger unit (Maxwell) was modified to operate on 10-V trigger pulses provided by a delay generator (Hewlett-Packard, Model 8112A). The trigger unit contains a small semiconductor controlled rectifier (SCR) that drives an optoelectronic coupler that isolates the input from the high-voltage circuitry. (The optoelectronic couplers were incorporated to isolate operators and equipment from any high voltage inadvertently coupled through the transformer.) The optoelectronic coupler, in turn, drives a relatively high-current SCR. This SCR was then used to pulse the grid of a 2D21 thyratron. The thyratron tube switched a 0.1-μF capacitor, charged to 250 V, across the primary of a small 1:100 pulse transformer. The secondary produced about 25,000 V, generating a spark at the trigger electrode. The thyratron was added since the secondary to primary capacitance of the transformer could couple the voltage spike produced by the capacitor discharge back into the electronics, and possibly damage solid state devices.

A pair of long leads connected the thyratron trigger switch and charging supply to the 0.1-μF capacitor and pulse transformer. The trigger capacitor and pulse transformer were mounted on a Bakelite cross member just above the spark gap. The capacitor was in series with the transformer primary and charged in about 1 s by the high-impedance supply. The thyratron was connected across the power supply and, upon being pulsed, rapidly discharged the capacitor through the transformer.

Although this triggering design proved convenient and reliable, it did pose a potential safety hazard—namely, that upon completing the discharge circuit, the trigger electrode, which was originally at ground potential, assumed the high voltage developed across the foil. Since the electrode was connected by a length of coaxial cable to the trigger transformer, the secondary winding of this transformer assumes this high voltage. This is not a problem as long as the insulation of the transformer does not fail. However, if the insulation fails, the voltage will be applied to the circuitry that activates the transformer. Therefore precautions were taken to robustly ground the equipment and to avoid direct operator contact.

A-9. Reduction of Electrical Noise. When any quiescent electrical circuit is suddenly discharged, spurious voltage transients (electrical noise) are almost always coupled into surrounding objects and instruments, creating problems in synchronization and measurement. The large, fast

transient associated with the explosion of a metallic foil presents a particularly difficult challenge for the experimenter. To combat entry of electrical noise into the measurement and triggering circuits, the following steps were taken.

(1) A single, central point was chosen to which all the equipment was grounded. Leads radiating from a single point do not form loops that can support currents produced by changing magnetic fields.

(2) The third prong ground on all recording equipment was broken by the use of a three-to-two prong adapter with its grounding lead removed. The third-prong grounds the equipment to the power-line ground, which is different from the central ground. Since earth serves to connect the central and power line grounds at one end and the equipment chassis on the other end, a ground loop is formed. Changing magnetic fields induce noise-producing currents in such loops. Breaking the power line ground interrupts this loop, yet the equipment is still properly grounded.

(3) Screening, tied directly to the capacitor, enclosed the entire discharge system. Screening intercepts electric fields that exist between the high-voltage elements of the gun-capacitor system and ground. If the screen was not employed, equilibration of the field-induced charges produced when the gun is fired would result in oscillatory current flow in the ground leads, etc. The conducting wires of the screen confine such currents.

(4) Recording equipment power cords and instrument-to-instrument leads were wound onto ferrite toroids. The path to ground broken by the three-to-two prong adapter is paralleled by other paths that can complete the earth-to-ground loop. One of these is the path through the recording device power transformers and the power line neutral lead to ground. Another is instrument-to-instrument (trigger) leads. The toroid wrap lessens this effect by increasing the impedance of the path.

(5) All possible separation was maintained between the recording devices and grounded surfaces. The capacitance between the recording device chasses and ground provides another path forming the earth-to-ground loop. Maintaining separation decreases the capacitance, thereby reducing this effect.

Another method of reducing noise is to enclose current and voltage measurement (coaxial) signal cables in the oscilloscope-grounding braid sleeve. By enclosing the signal leads in the sleeve, the braid and the cable shields cannot form a loop, lessening the current flowing in the shields. This can be important since the portion of shield carrying remnant ground circuit currents is also a portion of circuit supporting the small measurement signal currents. The impedance of this is common to the two circuits, and any voltage produced in it by the current in one circuit is added to the voltages in the other circuit. This common impedance is the major process coupling noise in a coaxial measuring circuit.

NO. OF COPIES	ORGANIZATION
2	DEFENSE TECHNICAL INFORMATION CENTER DTIC DDA 8725 JOHN J KINGMAN RD STE 0944 FT BELVOIR VA 22060-6218
1	HQDA DAMO FDQ DENNIS SCHMIDT 400 ARMY PENTAGON WASHINGTON DC 20310-0460
1	DPTY ASSIST SCY FOR R&T SARD TT F MILTON RM 3EA79 THE PENTAGON WASHINGTON DC 20310-0103
1	OSD OUSD(A&T)/ODDDR&E(R) J LUPO THE PENTAGON WASHINGTON DC 20301-7100
1	CECOM SP & TRRSTRL COMMCTN DIV AMSEL RD ST MC M H SOICHER FT MONMOUTH NJ 07703-5203
1	PRIN DPTY FOR TCHNLGY HQ US ARMY MATCOM AMCDCG T M FISETTE 5001 EISENHOWER AVE ALEXANDRIA VA 22333-0001
1	PRIN DPTY FOR ACQUSTN HQ US ARMY MATCOM AMCDCG A D ADAMS 5001 EISENHOWER AVE ALEXANDRIA VA 22333-0001
1	DPTY CG FOR RDE HQ US ARMY MATCOM AMCRD BG BEAUCHAMP 5001 EISENHOWER AVE ALEXANDRIA VA 22333-0001

NO. OF COPIES	ORGANIZATION
1	INST FOR ADVNCD TCHNLGY THE UNIV OF TEXAS AT AUSTIN PO BOX 202797 AUSTIN TX 78720-2797
1	USAASA MOAS AI W PARRON 9325 GUNSTON RD STE N319 FT BELVOIR VA 22060-5582
1	CECOM PM GPS COL S YOUNG FT MONMOUTH NJ 07703
1	GPS JOINT PROG OFC DIR COL J CLAY 2435 VELA WAY STE 1613 LOS ANGELES AFB CA 90245-5500
1	ELECTRONIC SYS DIV DIR CECOM RDEC J NIEMELA FT MONMOUTH NJ 07703
3	DARPA L STOTTS J PENNELLA B KASPAR 3701 N FAIRFAX DR ARLINGTON VA 22203-1714
1	US MILITARY ACADEMY MATH SCI CTR OF EXCELLENCE DEPT OF MATHEMATICAL SCI MDN A MAJ DON ENGEN THAYER HALL WEST POINT NY 10996-1786
1	DIRECTOR US ARMY RESEARCH LAB AMSRL CS AL TP 2800 POWDER MILL RD ADELPHI MD 20783-1145
1	DIRECTOR US ARMY RESEARCH LAB AMSRL CS AL TA 2800 POWDER MILL RD ADELPHI MD 20783-1145

NO. OF
COPIES ORGANIZATION

3 DIRECTOR
US ARMY RESEARCH LAB
AMSRL CI LL
2800 POWDER MILL RD
ADELPHI MD 20783-1145

ABERDEEN PROVING GROUND

4 DIR USARL
AMSRL CI LP (305)

NO. OF COPIES	ORGANIZATION
1	PM SRVBLTY SYSTM SFAE ASM SS M M RYZYI WARREN MI 48397-5000
1	CDR USA ARDEC AMSTA AR AEE B D DOWNS PICATINNY ARSENAL NJ 07806-5000
2	CDR USA ARDEC AMSTA AR AEE WW P LU B FISHBURN PICATINNY ARSENAL NJ 07806-5000
1	CDR USA ARDEC AMSTA AR EE WW J LANNON PICATINNY ARSENAL NJ 07806-5000
1	BATTELLE D TROTT 505 KING AVE COLUMBUS OH 43201
1	DIR LANL D IDAR PO BOX 1633 LOS ALAMOS NM 87545
	ABERDEEN PROVING GROUND
30	DIR ARL AMSRL WM P, W CIEPICLA A HORST M SMITH AMSRL WM PA, A BIRK T COFFEE J COLBURN J DESPIRITO C LEVERITT T MINOR S RAY G WREN AMSRL WM PB, P PLOSTINS

NO. OF COPIES	ORGANIZATION
	AMSRL WM PC, R BEYER S BUNTE B FORCH K MCNESBY M J MCQUAID (5 CP) R PESCE-RODRIGUEZ AMSRL WM T, W MORRISON AMSRL WM TC, P BAKER R FREY G GIBBONS W LAWRENCE D PILARSKI J STARKENBERG J WATSON

INTENTIONALLY LEFT BLANK.

REPORT DOCUMENTATION PAGE

Form Approved
OMB No. 0704-0188

1. AGENCY USE ONLY *(Leave blank)*	2. REPORT DATE	3. REPORT TYPE AND DATES COVERED
	March 1998	Final, May 94 - Mar 96

4. TITLE AND SUBTITLE
Real-Time Laser-Based Detection of Chemical Intermediate Formation in Liquid Propellant XM46 Shock-Loaded via an Electric Gun

5. FUNDING NUMBERS
1L162618AH80

6. AUTHOR(S)
M. J. McQuaid, H. Burden, and W. Lawrence

7. PERFORMING ORGANIZATION NAME(S) AND ADDRESS(ES)
U.S. Army Research Laboratory
ATTN: AMSRL-WM-BD
Aberdeen Proving Ground, MD 21005-5066

8. PERFORMING ORGANIZATION REPORT NUMBER
ARL-TR-1625

9. SPONSORING/MONITORING AGENCY NAMES(S) AND ADDRESS(ES)

10.SPONSORING/MONITORING AGENCY REPORT NUMBER

11. SUPPLEMENTARY NOTES

12a. DISTRIBUTION/AVAILABILITY STATEMENT
Approved for public release; distribution is unlimited.

12b. DISTRIBUTION CODE

13. ABSTRACT ***(Maximum 200 words)***

This report describes the development and results of an experiment designed to obtain real-time spectroscopic evidence of chemical intermediate formation in shock-loaded liquid propellant (XM46). Shock loads were produced by impacting small (<1 cm^3) XM46 samples with thin (0.075–0.375 mm) Mylar flyer plates. The flyer plates were accelerated to velocities near 1 mm/μs by the expansive forces of an exploding foil, a technique referred to as an "electric gun." A detailed description of the design of the gun developed for this study is provided. The performance of the apparatus was characterized in visualization experiments and via CTH (hydrocode) simulations. In spectroscopy experiments, the XM46 samples were probed at various delays following impact via laser-induced Raman scattering and fluorescence. A signature that may be attributable to NO_2 was observed, but cavitation was induced ahead of the shock wave, limiting our ability to establish the role of chemical intermediate formation in the shock-induced initiation of XM46. Issues in configuring experiments to detect chemical intermediate formation in shock-loaded samples via real-time, optically based spectroscopies are discussed.

14. SUBJECT TERMS
electric gun, XM46, shock-loading diagnostics

15. NUMBER OF PAGES
50

16. PRICE CODE

17. SECURITY CLASSIFICATION OF REPORT	18. SECURITY CLASSIFICATION OF THIS PAGE	19. SECURITY CLASSIFICATION OF ABSTRACT	20. LIMITATION OF ABSTRACT
UNCLASSIFIED	UNCLASSIFIED	UNCLASSIFIED	UL

NSN 7540-01-280-5500

Standard Form 298 (Rev. 2-89)
Prescribed by ANSI Std. 239-18 298-102

INTENTIONALLY LEFT BLANK.

USER EVALUATION SHEET/CHANGE OF ADDRESS

This Laboratory undertakes a continuing effort to improve the quality of the reports it publishes. Your comments/answers to the items/questions below will aid us in our efforts.

1. ARL Report Number/Author ARL-TR-1625 (McQuaid) Date of Report March 1998

2. Date Report Received _____

3. Does this report satisfy a need? (Comment on purpose, related project, or other area of interest for which the report will be used.) _____

4. Specifically, how is the report being used? (Information source, design data, procedure, source of ideas, etc.) _____

5. Has the information in this report led to any quantitative savings as far as man-hours or dollars saved, operating costs avoided, or efficiencies achieved, etc? If so, please elaborate. _____

6. General Comments. What do you think should be changed to improve future reports? (Indicate changes to organization, technical content, format, etc.) _____

CURRENT ADDRESS

Organization

Name E-mail Name

Street or P.O. Box No.

City, State, Zip Code

7. If indicating a Change of Address or Address Correction, please provide the Current or Correct address above and the Old or Incorrect address below.

OLD ADDRESS

Organization

Name

Street or P.O. Box No.

City, State, Zip Code

(Remove this sheet, fold as indicated, tape closed, and mail.)

(DO NOT STAPLE)